Desalination and Water Treatment
www.deswater.com

doi: 10.5004/dwt.2020.25965

197 (2020) 424–437
September

Royal blue dianix CC dye adsorption onto biochars: kinetics, diffusion modeling, equilibrium and thermodynamic adsorption data

Mylena Junqueira Pinto Brito, Jessica Ferreira Borges, Thainá Peixoto de Oliveira, Mateus Pereira Flores Santos, Evaldo Cardozo de Souza Júnior, Leandro Soares Santos, Renata Cristina Ferreira Bonomo, Cristiane Martins Veloso*

Process Engineering Laboratory, State University of Southwest Bahia, Itapetinga, BA, Brazil, CEP 45700-000, Tel. +55-77-3261-8659, emails: crisvel@uesb.edu.br (C.M. Veloso), mylena_junqueira@hotmail.com (M.J.P. Brito), jessicajfborges@gmail.com (J.F. Borges), thay.oliveira14@hotmail.com (T.P. de Oliveira), mateuspfloress@outlook.com (M.P.F. Santos), evaldocsj@yahoo.com.br (E.C. de Souza Júnior), leosoaressantos@yahoo.com.br (L.S. Santos), bonomorcf@yahoo.com.br (R.C.F. Bonomo)

Received 11 November 2019; Accepted 9 April 2020

ABSTRACT

This work presents a detailed analysis of the adsorption process of royal dianix CC blue dye on biochars, synthesized from the bark of cupuaçu, a lignocellulosic residue generated by the food industry. The biochars were activated with KOH or H_3PO_4 and carbonized at a temperature of 450°C. The kinetic parameters, the diffusion coefficients, the equilibrium data, and the thermodynamic parameters of the dye adsorption were also determined. The chemical and physical properties of the porous materials were affected by the activating agent used. The adjustment of the kinetic models to the experimental data suggested that the dye adsorption onto both biochars occurred predominantly by chemisorption, which was controlled by the external mass transfer. The acid and basic carbons presented a maximum adsorption capacity of 98.45 and 66.95 mg g^{-1}, respectively. The negative values of Gibbs free energy and enthalpy indicate that the adsorption is spontaneous and exothermic.

Keywords: Biomass residues; Diffusion modeling; Textile dyes; Adsorption mechanism

1. Introduction

Several industrial segments stand out in the environmental scenario as major polluters, with a strong emphasis on the textile sector due to the volume of effluents generated, characterized by the heavily colored synthetic dyes, which do not fully bind to the fiber during the dyeing process [1].

The presence of dyes in effluents affects aesthetics, water transparency, and gas solubility in water bodies, reducing the capacity of water bodies to regenerate due to the lower sunlight penetration and consequent alteration of photosynthesis. Dyes can also cause allergy, dermatitis, and skin irritation, and some dyes have also carcinogenic and mutagenic potential [2–4].

Due to their chemical structure, the synthetic dyes are characterized by having high resistance to conventional treatment processes, like flocculation and coagulation, and aerobic biodegradation. In this sense, alternative methods have been investigated for effluent dye removal, including electrodialysis, reverse osmosis, ultrafiltration, and adsorption [5–7].

* Corresponding author.

The adsorption stands out as a viable technological alternative, due to its simplicity, less processing time, efficiency, and flexibility, and can be used to remove a wide range of pollutants. It consists of a mass transfer operation, in which the compounds in a fluid phase are transferred to a solid phase. The compounds retained onto the solid surface are called adsorbates, while the solid phase is called adsorbent [8,9]. Whereas the adsorbed components concentrate on the outer surface, the greater the surface area per unit mass of the solid, the more favorable the adsorption will be, thus the adsorbents are generally porous solids [10,11].

The biochar, an activated carbon obtained from biomass, is one of several adsorbent matrixes used in many industrial applications. It consists of carbonaceous material, with a highly developed porous structure and the presence of heteroatoms (O, N, and H) on its surface, which are obtained by chemical or physical activation of the biomass [12,13]. The synthesis consists of two main steps: carbonization and activation. Carbonization consists of the thermal treatment of the biomass in an inert atmosphere or not, at temperatures which may vary from 400°C to 900°C. Activation, in turn, consists of subjecting the material to secondary reactions, aiming at the development of porosity, increase in specific surface area, and superficial functional groups, which can occur by physical or chemical processes. The characteristics of the biochars are influenced, in particular, by the precursor carbon and the activation method used [10,14,15].

The products used in the production of carbon are compounds with high carbon value and low inorganic content, as well as solid agroindustrial residues (bark and seeds, wood, and bagasse) [12,16]. The production of biochar from biomass residues may be an attractive alternative since it allows the generation of products with high added value and adequate physicochemical properties [10,17]. Thus, studies on the potential of new lignocellulosic materials for carbon production is of the utmost importance.

The cupuaçu tree (*Theobroma grandiflorum*) is a fruit tree of the tropical forest, native to the Brazilian Amazon. The relative composition of the fruit (mass) is on average 46% bark, 36% pulp, and 18% seeds. Cupuaçu pulp is mainly used in the production of juices, ice cream, and desserts in the food industry, while the seeds can be used in the preparation of an analog to chocolate [18]. In contrast, cupuaçu bark is generally considered as a by-product in the food industry, with no economic value. The inadequate disposal of this residual biomass in soils and natural waters can lead to the production of various chemical compounds and microorganisms that can contaminate the environment [19]. Thus, the conversion of this residue into biochar may be a promising alternative to minimize the environmental problems and to reduce the costs of manufacturing of this material.

Due to the above, this work had the objective of producing biochars from the food agroindustrial residues (cupuaçu bark) and to evaluate the ability of the materials produced to adsorb the royal dianix CC blue dye. In addition, a detailed analysis of the entire process including kinetic study, consistent mathematical modeling of the dye diffusion process in the porous materials, and the determination of the thermodynamic parameters equilibrium data were performed.

2. Materials and methods

2.1. Synthesis of the biochars

Cupuaçu bark was used as a precursor material (PM) for the synthesis of the biochar. The PM was washed in running water to remove fruit residues and dried at 105°C for 24 h. They were then ground in a knife mill and sieved in a 420 μm sieve. For the synthesis process, the chemical activation of the lignocellulosic material was performed, followed by carbonization, with modifications as a function of the activation agent used.

Biochars were prepared by chemical activation according to the methodology described by Brito et al. [10] and Santos et al. [20], with modifications. The PM was impregnated with phosphoric acid (85% P.A.-CAS7664-38-2) or potassium hydroxide (CAS226-37-39) in the impregnation ratio of 1:1 and kept in a drying oven at 105°C for 48 h. The carbonization step was performed in a muffle furnace at 450°C (heating rate of 5°C min^{-1}) under nitrogen flow (50 mL min^{-1}) for 60 min. After this step, the excess of the activating agent was removed in the washing step, and the biochars were dried and sieved. The yield in biochar was calculated by Eq. (1).

$$\text{Yield}(\%) = \left(\frac{W_f}{W_0}\right) \times 100 \quad (1)$$

where W_C and W_p (g) are the weight of the biochar and the dried PM, respectively.

2.2. Characterization of the cupuaçu bark and biochars

The cupuaçu bark was characterized for the composition in lignocellulosic material (lignin, cellulose, and hemicellulose) and ash content. The concentrations of neutral detergent fiber and acid detergent fiber were determined according to the methodology described by Van Soest et al. [21]. The lignin content was determined by the sulfuric acid method (72%). Cellulose, hemicellulose, and ash contents were quantified following the protocols described by AOAC [22], in which all chemical constituents are reported on a dry matter basis. The functional groups were evaluated by Fourier-transform infrared spectroscopy (FTIR), using the attenuated total reflectance in the infrared region of 4,000–500 cm^{-1} in an Agilent Cary 630 FTIR spectrometer (Agilent Technologies Inc., Santa Clara, CA, USA). The pH of the zero charge point (pHpzc) of biochars was evaluated as described by Regalbuto and Robles [23]. The isotherms of adsorption/desorption of nitrogen at 77 K were obtained in a Micrometrics ASAP 2420 (Micromeritics Instrument Corporation, Norcross, GA 30093, USA), according to the methodology described by Brito et al. [10]. The morphology of the carbons samples was so analyzed in a scanning electron microscope equipped with EDS (Thermo scientific NSS Spectral Imaging, JEOL Model, JMS – 6610, Tokyo, Japan), according to the method described by Santos et al. [20].

2.3. Adsorption experiments

The royal dianix CC blue dye, donated by a textile industry located in the state of Bahia-Brazil, was used as the

model molecule for the study of the adsorptive process on biochars. The influence of the initial pH (3.0, 5.0, 7.0, and 9.0) of the dye solution on the adsorptive capacity of the porous materials, kinetic and adsorption isotherms of adsorption was evaluated. The experiments were conducted as follows: 5 ml of the dye solution were placed in tubes containing 0.25 mg of each biochar and kept under constant stirring on an orbital shaker at 20 rpm, for a predetermined time, pH and temperature. The pH of the solution was adjusted with monobasic or bibasic sodium phosphate buffer solution (200 mg L^{-1}). After each assay, the tubes were centrifuged (3,500 rpm) for 10 min. The concentration of the dye in the supernatant was determined by direct reading in a UV/Visible spectrophotometer (Quimis, Diadema, SP, Brazil) at the wavelength of 624 nm. All experiments were made in triplicate and the adsorptive capacity (q_e, mg/g) of the biochars was calculated using Eq. (2).

$$q_e = \frac{VC_{in} - VC}{m_{ads}} \tag{2}$$

where V is the volume of the solution (mL), C_{in} initial concentration of the solution (mg L^{-1}), C is the concentration of the solution (mg L^{-1}) at equilibrium, and m_{ads} is the mass of the adsorbent (g).

In order to understand the dynamics of adsorption of the dye in the biochars, as well as the adsorbate/adsorbent interaction, the kinetic models (pseudo-first-order, pseudo-second, Elovich, and intra-particle diffusion) and adsorption isotherms (Langmuir and Freundlich) were adjusted to experimental data. Nonlinear models and the linear model for intraparticle diffusion were fitted to the experimental data using sigma plot student software. The models were evaluated according to the determination coefficient (R^2) and the root means square error (RMSE), according to Eq. (3).

$$\text{RQEM} = \sqrt{\frac{\Sigma\left(\bar{Y} - Y\right)^2}{N}} \tag{3}$$

where $\bar{Y}$ is the variable estimated by the model, Y is the variable obtained experimentally, and N is the number of observations.

3. Results and discussion

3.1. Cupuaçu bark composition

The lignocellulosic material (cupuaçu bark) contains a low ash content (2.67%, on a dry basis) and lignocellulosic content of 43.40% cellulose, 32.29% lignin, and 12.53% hemicellulose, with a cellulose/lignin ratio of 1.34. The lignocellulosic content determines, to some extent, the physical properties of carbon. Studies have shown that precursors with cellulose and hemicellulose contents higher than lignin can be more easily activated, consequently increasing the porosity of the carbon produced. This result is due to the cellulose and hemicellulose are volatile fractions removed during the pyrolysis and activation processes, leading to a pore development, whereas lignin, which confers rigidity to the biomass matrix, is the constituent with the lower capability to volatilize [24,25].

3.2. Yield and characterization of the biochars

The yield of the synthesis process and the characterization of the biochars are shown in Table 1. The synthesis yield of the biochar is an important parameter, which indicates the production viability of the adsorbent from a given precursor. In this study, the activation with H_3PO_4 (BCP) led to the development of an adsorbent with higher yield when compared to the activation with KOH (BCK). The high yield observed for the acid activation is due to the dehydrogenation reactions that inhibit the formation of aromatic hydrocarbons (tar) and reduce the production of other volatile products during carbonization [26]. Moreover, phosphoric acid can form a protective layer in the pore structure, generating phosphate, and polyphosphate esters that prevent excessive adsorption of the porous material, resulting in a higher yield [27]. The activation with KOH, in turn, leads to the formation of volatile compounds and light gases at lower temperatures before the activation of chemical reactions, thus leading to lower yields [10,28]. The impregnation ratio also provided a more rapid activation, accompanied by the release of volatiles.

Both biochars exhibited ash content higher than the precursor. It is known that phosphoric acid and potassium hydroxide promotes the biomass dehydration during the activation step, while the carbonization leads to the conversion of some carbonaceous materials into inorganic compounds, which are not removed in the washing step, leading to an increase in ash content of the porous material [6].

The FTIR spectra of the cupuaçu bark and the synthesized biochars are presented in Fig. 1. In the spectra of PM can be observed various bands characteristic of lignocellulosic materials. A broad adsorption region around 3,319 cm^{-1}, corresponding to the stretching vibrations of hydroxyl or carboxyl groups present in cellulose structure, the main component of the cupuaçu bark. The band at 2,098 cm^{-1} related to carbonyl stretching (C=O). The peak around 1,615 cm^{-1}, which is generally associated with C=O vibrations of carboxymethyl cellulose. The peak at 1,236 cm^{-1} corresponding to the aromatic ring vibration of lignin (guaiacyl rings), and an intense peak at 1,019 cm^{-1} associated with the C–O

Table 1
Yield and characterization of the biochars

Parameters	Sample	
	BCP	BCK
Yield (%)	31.90	11.90
Ash (%)	7.58	4.24
pHpzc	4.8	6.7
Surface area ($m^2 g^{-1}$)	913	73
Pore diameter (nm)[a]	3.683	7.740
Mesopore volume ($cm^3 g^{-1}$)	0.318	0.042
Micropore volume ($cm^3 g^{-1}$)	0.150	0.016

[a]Maximum pore size distribution

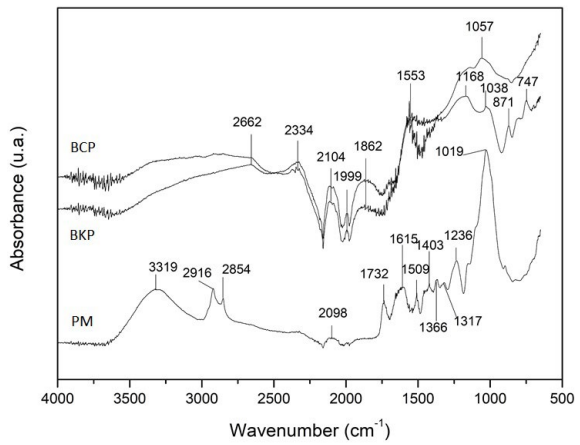

Fig. 1. FTIR of the cupuaçu bark and the biochars.

stretching of cellulose, hemicellulose, and lignin or C–O–C stretching of cellulose and hemicellulose. Finally, a small shoulder was observed at 898 cm^{-1} corresponding to the β-glycosidic bonds between the sugar units of hemicellulose and cellulose [29–31].

Concerning the spectra of the biochar, the activation and carbonization processes were responsible for a reduction in the number of bands, as observed for the peaks at 2,916 and 2,854 cm^{-1}, indicating the decomposition of the lignocellulosic constituents during the synthesis process. The appearance of bands and peaks associated with other functional groups was also observed, characteristic of carbonaceous materials, emphasizing the vibrations of the carbon skeleton, characteristic of biochars, at 1,600 cm^{-1} corresponding to the symmetrical stretching of the C=C of aromatic rings [11]. The different activating agents led to the emergence of distinct bands on the biochar surface. For BCP, bands at 1,168 and 1,038 cm^{-1} were observed, characteristic of P=O in phosphate ester, and O–C bond in P–O–C and P=OOH [16,32] and a lower peak at 871 cm^{-1}, related to CH curvature of aldehydes, pyranose compounds, and benzene derivatives [33]. For BCK, a band at 1,057 cm^{-1} was observed, corresponding to stretches of glycosidic bonds (COC) present in the structure of the lignocellulosic components, evidencing that this material underwent minor structure modifications when compared to the BCP [10]. The knowledge of the functional groups of the porous materials is important to understand the adsorption mechanisms.

The surface charge of the biochars was evaluated by determination of the point of zero charges (pHpzc). At this pH range, the carbon surface presents zero residual electric charges. When the material comes into contact with a solution with pH lower than the pHpzc, its surface is positively charged, with a greater removal efficiency of anionic materials. When the solution has a pH value higher than pHpzc, the surface is negatively charged, preferentially adsorbing cationic compounds [3,12]. The different ionization behavior observed in the carbons (Table 1) may be due to the chemical structure of the activating agent used. Activation with H_2PO_4 led to the synthesis of carbon with oxygenated groups on its surface, associated with carboxylic acids, alcohols, phenols, and esters, as observed in the FTIR spectra, which confers acidic characteristics. This behavior was not observed for basic activation.

N_2 sorption isotherms and pore distribution of the biochars are shown in Fig. 2. In accordance with the International Union of Pure and Applied Chemistry classification, the N_2 sorption isotherms of both biochars can be classified as type IV, that is, they represent porous solids with micro and mesopores. The hysteresis cycles, observed in both isotherms, is attributed to the capillary condensation mechanism of N_2 in the mesopores [8,34]. It is also possible to verify that the volume of N_2 adsorbed by the sample BCP was higher than that of the sample BCK, indicating a larger pore volume available for the adsorption phenomenon, and consequently a larger surface area (S_{BET} (BET – Brunauer–Emmett–Teller method)). Moreover, the adsorption and desorption curves of the carbon BCK are not found in low relative pressure values, as observed for the BCP, probably due to the pore distribution of these materials. The carbon BCK exhibited a narrower pore distribution in the mesopore range, with a pore widening in the region of larger pores, while the carbon BCP exhibited a more evident tendency of micropore formation. In the adsorption mechanism, a good ratio between mesopores and micropores is required, once the adsorbents may be able to rapidly diffuse the molecules inside the carbon and to access the micropores, where the adsorption occurs to a great extent [6,7,33].

In Table 1 are shown the results of the texture characterization of the biochars. A material with greater S_{BET}, total pore volume, and micropore volume were obtained when the activation with phosphoric acid was used. This behavior can be due to the different reaction mechanisms of the activating agents employed. In relation to the mechanism of action involving H_3PO_4, it is known that this chemical acts as an acid catalyst, leading to a bond rupture of the lignocellulosic components, the formation of crosslinks via cyclization and condensation reactions, in addition to combining with organic species to form phosphate and polyphosphates bridges, which connects and crosses the biopolymer fragments. The addition (or insertion) of phosphate groups initiates a dilation process leaving the matrix in an expanded state with an accessible pore structure [35,36]. These chemical reactions take place at mild activation temperatures, and the concomitant development of microporosity is usually observed at a temperature between 150°C to 350°C. A further increase in temperature results in the formation of mesopores, mainly through enlargement of the existing micropores. In addition, after the activation process, water from the washing step removes the phosphates formed, leaving a void space comprising a micropore with a volume corresponding to the compound removed [35,37].

The reaction mechanism between KOH and the constituents of the carbon precursor evolves dehydration and oxidation steps with the formation of K_2O and K_2CO_3, which are transformed into metallic potassium [Eq. (4)] [38], which diffuses between the layers of the structural graphene and enlarges them.

$$4KOH + C \rightarrow 4K + CO_2 + 2H_2O \quad (4)$$

The last step of the carbon synthesis is washing the material with HCl (0.2 mol L^{-1}) and water to remove residual

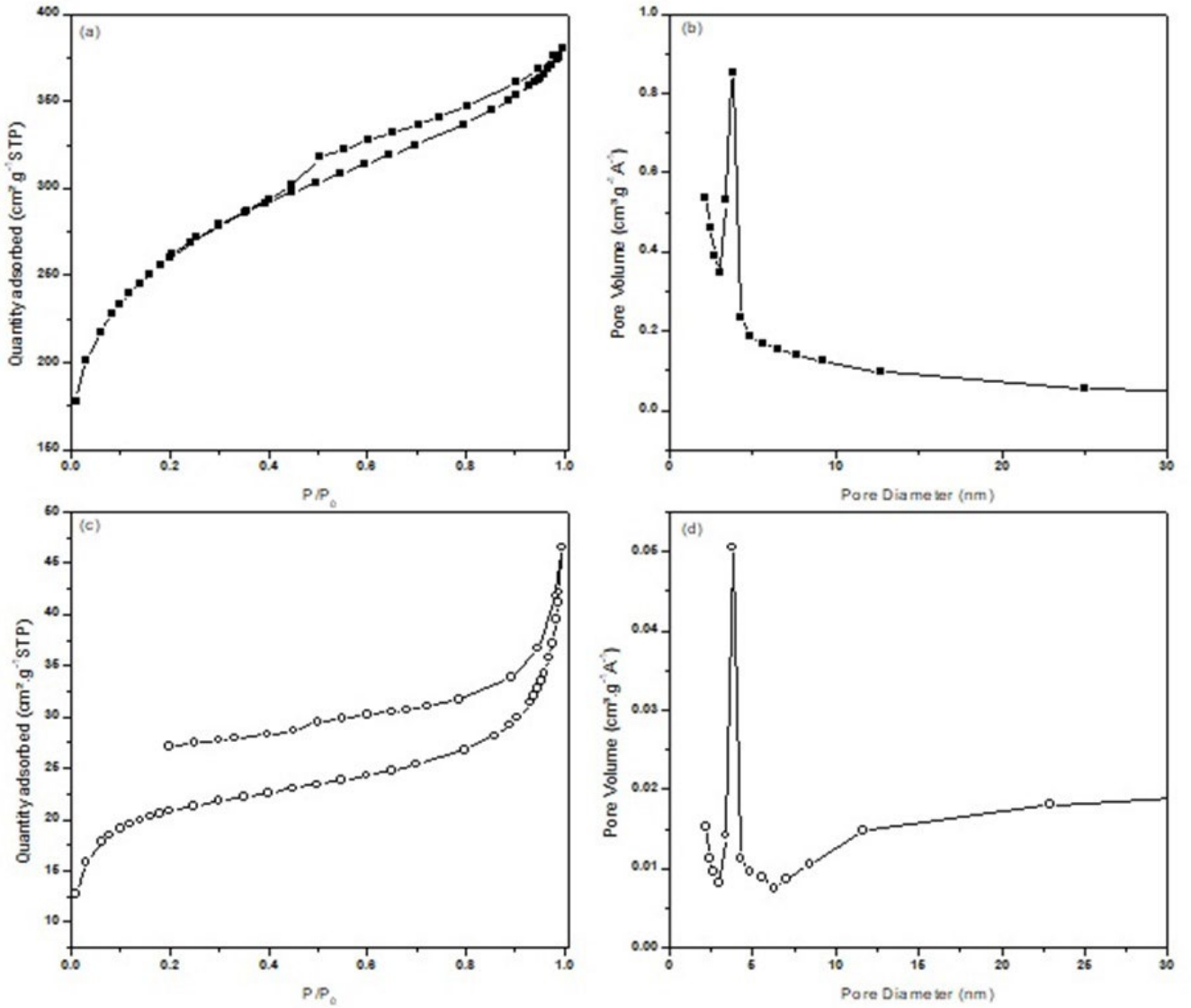

Fig. 2. N_2 sorption isotherms and pore distribution of biochar BCP (a and b) and BCK (c and d).

K, K_2O, K_2CO_3, and KOH from the graphene layers. The structures of the pseudolamellar graphite cannot return to their original non-porous structure, resulting in the development of porosity and an increase in the surface area [39–41]. However, it is worth noting that these reactions occur more effectively at temperatures higher than 400°C) and become thermodynamically viable when the carbonization temperature is higher to the boiling point of potassium (762°C) [7,42]. The temperature used in the carbon synthesis with KOH was 450°C, thus it was not sufficient to promote the greater porosity development and increase the carbon S_{BET}.

The effect of the chemical agent used for the impregnation of the carbon PM on the texture characteristics of the synthesized biochars was also evaluated by scanning electron microscopy (SEM). A porous structure, with different morphologies, was observed for both materials (Fig. 3). The BCP (Fig. 3a) has an irregular structure with well-developed pores, with large slits, which extended to the inside of the adsorbent. Thus, more channels were formed, which contributed to increase the access to micro and mesopores, thus increasing their adsorptive capacity [43]. The sample BCK (Fig. 3b) presented a spongy structure, with light spots and denser nuclei. The formation of this type of structure is due to the synthesis conditions, which did not allow more effective hydrolysis of the lignocellulosic structures, interfering in the development of the porosity and consequently the increase in S_{BET}, as discussed.

3.3. Royal dianix CC blue dye adsorption process

The pH of the solution is an important variable that is studied in the adsorptive process since the variation of this parameter can promote changes in the surface charges of the adsorbate molecules and porous materials. [11] When the adsorption capacity (q) of the carbons was evaluated (Fig. 4), although dye adsorption was observed at all pH

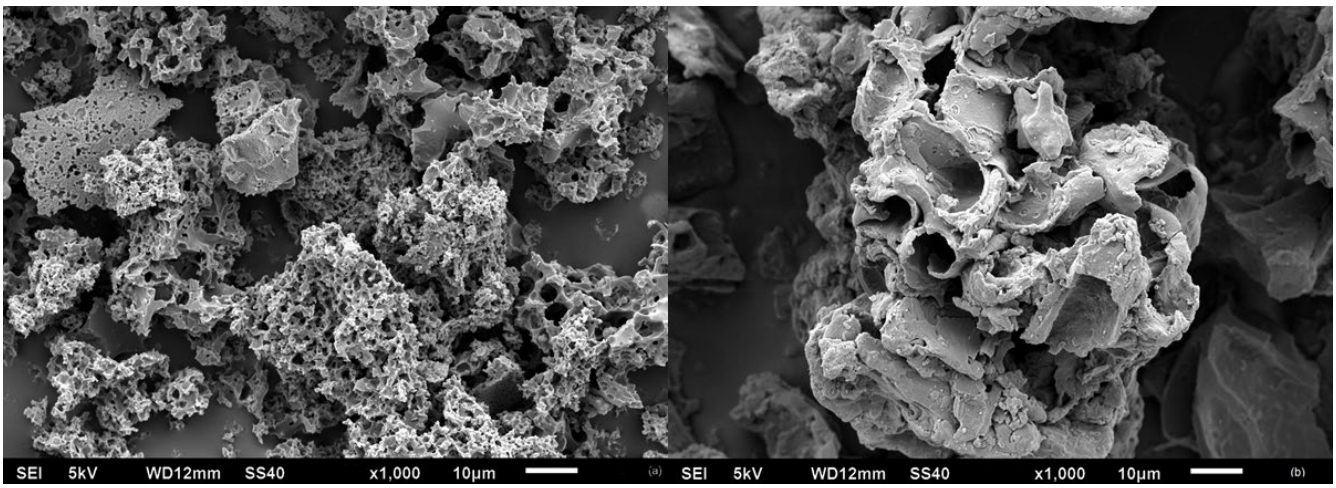

Fig. 3. SEM images of samples BCP (a) and BCK (b).

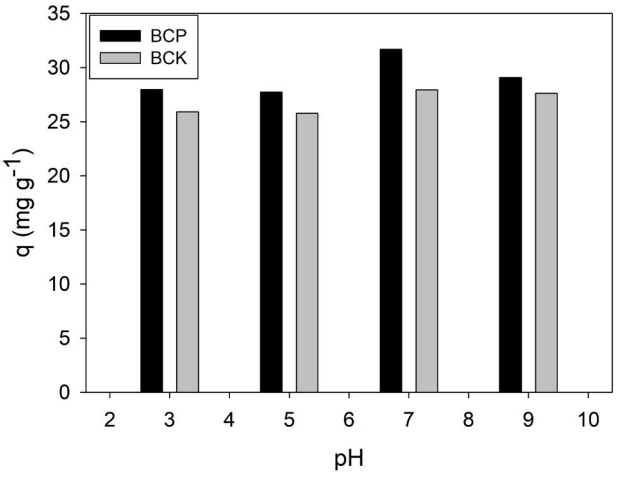

Fig. 4. Influence of the initial dye solution pH on the samples BCP and BCK adsorptive capacity (C_0 = 200 mg L^{-1}; T = 25°C; time = 24 h).

values, the higher adsorption capacity occurred at pH 7.0 for both biochars. At this pH value, the adsorbent surface has a negative charge (pH > pHpzc) and the dye surface presents positive and negative charges since the principal component of the dye (CI Disperse Green 9) is a molecule that has an amphoteric character [7]. Consequently, it is very stable and tends to suffer minimal lateral repulsions, thus favoring the formation of weak interactions: hydrogen bonds, van der Waals forces, and ion interactions, for example. The lower adsorptive capacity at pH above 7.0 is due to the positive residual charge of the dye at this pH value, due to the higher number of OH^- available in the mixture. Therefore, the ion interactions among the biochar and the dye are reduced, leading to a decrease in the adsorptive capacity of the biochars. As the sample BCP presented a greater number of acidic functional groups, this effect can be greater, leading to a lower dye removal when compared to the sample BCK. Therefore, the pH 7.0 was chosen to perform the other adsorption tests due to the higher adsorption capacity at this pH value for both carbons studied [44].

The kinetic adsorption studies are important to comprehend the adsorbent/adsorbate interactions, by determining parameters such as reaction order, the rate constant, and initial adsorption rate, as well as establishing the time required to reach equilibrium under certain conditions. In Figs. 5a and b are shown the results of the kinetic study of dye removal using the carbons BCP and BCK, respectively. A high removal rate from the fluid phase was observed, reaching the adsorption equilibrium within 60 and 90 min for BCP and BCK, respectively. The physical characteristics of the biochars, which directly affect the diffusion process of the dye molecules into the carbon pores and consequently, the time to reach equilibrium and amount of dye adsorbed.

To define an appropriate kinetic model capable of representing the dye adsorption onto the samples BCP and BCK, the pseudo-first-order [45], pseudo-second-order [46], and Elovich models [47], Eqs. (5)–(7), respectively, were fitted to the experimental data.

$$q_t = q_e\left[1 - e^{k_1 t}\right] \tag{5}$$

$$q_t = \frac{k_2 q_e^2 t}{1 + k_2 q_e t} \tag{6}$$

$$q_t = \frac{1}{\beta}\ln\left(1 + \alpha\beta t\right) \tag{7}$$

where q_e and q_t are the quantities adsorbed (mg g^{-1}) at equilibrium and at time t (min), respectively; k_1 is the pseudo-first-order adsorption rate constant (min^{-1}); k_2 is the pseudo-second-order rate constant (g mg^{-1} min^{-1}); α is initial adsorption rate constant (mg g^{-1} min^{-1}); β is desorption rate constant (g mg^{-1}).

In Table 2 the adjustment parameters of kinetics models are shown. The kinetic models fit satisfactorily to the experimental data, with high R^2 values and low RMSE

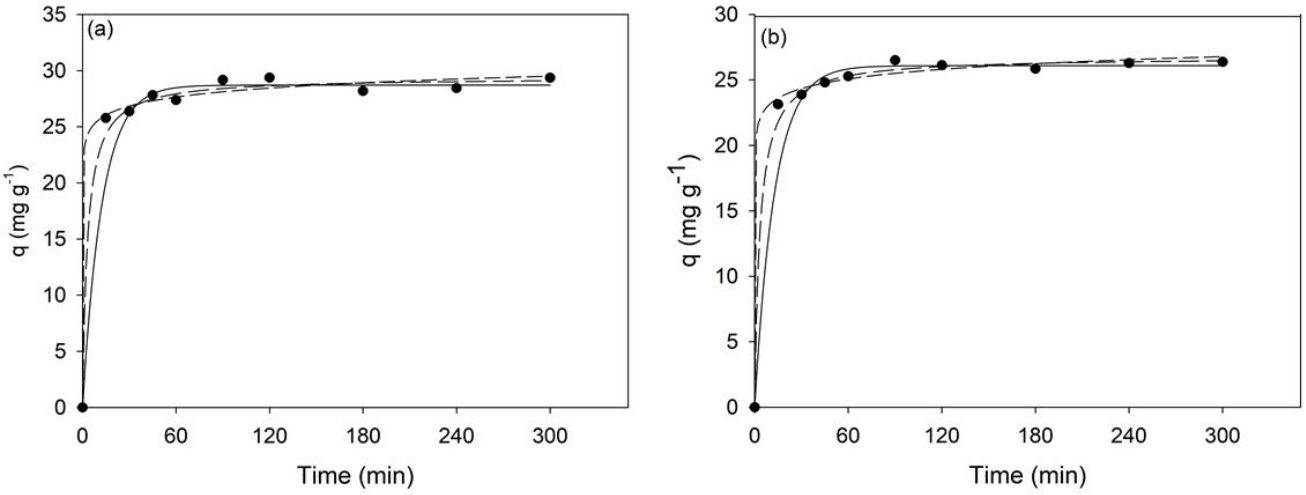

Fig. 5. Kinetics of dye adsorption in samples BCP (a) and BCK (b) and non-linear adjustments of pseudo-first-order (- -), pseudo-first-order (– –) and Elovich (•) models (C_0 = 200 mg L^{-1}; pH: 7.0; T = 25°C; time = 0–300 min).

Table 2
Kinetic and intra-particle parameters for royal dianix CC blue dye adsorption onto BCP and BCK

Kinetic constants	BCP	BCK
Pseudo-first-order rate model		
q_e (mg g^{-1})	28.706	26.081
k_1 (min^{-1})	0.080	0.077
R^2	0.996	0.998
RMSE	0.549	0.338
Pseudo-second-order model		
q_e	29.397	26.759
k_2 (mg g^{-1} min^{-1})	0.011	0.010
h_0 (mg g^{-1} min^{-1})	9.333	7.805
R^2	0.996	0.999
RMSE	0.526	0.288
Elovich		
α (mg g^{-1} min^{-1})	3.96×10^9	3.10×10^9
β (g mg^{-1})	1.157	1.060
R^2	0.995	0.997
RMSE	0.643	0.439
Morris–Weber rate model		
K_{ad} (mg $g^{-1}min^{-0.5}$)	2.976	1.794
C (mg g^{-1})	73.193	39.626
R^2	0.831	0.764

values, indicating that the predicted values approach the experimental ones. When evaluating the pseudo-first-order model, it can be inferred that there was no saturation of the active sites of the adsorbents, in other words, the amount of dye molecules is significantly lower than the number of available sites [45]. The second-order model was successfully employed to describe the adsorption kinetics of a variety of adsorbates in chemisorption processes, involving valence forces through the sharing or exchange of electrons between the adsorbent and adsorbate [48,49]. The satisfactory adjustment of the pseudo-second-order and Elovich models suggests the chemical adsorption as a limiting step, followed by the intraparticle diffusion phenomenon in the final stages [50]. When evaluating the parameters of the pseudo-second-order model, the adsorption equilibrium of the dye in the carbon BCK was reached faster when compared to the carbon BCP, once it presented a higher initial adsorption rate (h_0). This behavior may be associated with a lower surface adsorbent area, which implies a lower capacity to adsorb the dye molecules, as determined by the q_e for this matrix, consequently requiring a shorter time for the mass transfer process to reach equilibrium [7].

The coefficients α and β, determined by the Elovich model, represent the initial adsorption rate and the desorption coefficient, respectively [51]. As can be seen in Table 2, the high value of α compared to β, shows the viability of the adsorption process.

Kinetic models are used to examine the adsorption, chemical reaction, and mass transfer mechanisms. However, the definitive adsorption mechanism may not be obtained by these models, thus the intra-particle diffusion models, including the intra-particle diffusion Weber and Morris model [52] and Boyd's kinetic model [53] should be used.

The mass transfer mechanism of the adsorption process can be described by three consecutive steps: solute transport of the solution through the liquid film to the outer surface of the adsorbent (diffusion in the film), diffusion of the solute in the pore of the adsorbent, and adsorption of solute onto the inner surface of the adsorbent pores [54,55]. The quantitative treatment of experimental data reveals a predominant role of a particular step that governs the adsorption rate. As reported by Mohan et al. [56], the third step does not represent the limiting step of the process because it is very fast, thus the film diffusion or the particle diffusion must govern the overall process. According to Weber and Morris [52], if the intra-particle diffusion is the determinant of velocity,

the adsorption removal varies linearly with the square root of time [57]. In this case, it is considered that the diffusion within the solid particle occurs slowly, limiting the process. Thus, surface diffusion happens gradually and linearly, and the model can be well represented by Eq. (8).

$$q_t = K_{ad} t^{1/2} + C \tag{8}$$

where q_t is the amount of adsorbate adsorbed on the solid phase (mg g^{-1}) at time t (min), K_{ad} intra-particle diffusion coefficient (mg g^{-1} $min^{-0.5}$), and C constant related to diffusion resistance (mg g^{-1}).

The Boyd model, in turn, was proposed to determine if the external transport or intra-particle diffusion is the limiting step [58]. According to this model, the fraction of solute adsorbed at a certain time t can be determined by Eqs. (9) and (10).

$$F = 1 + \left(\frac{6}{\pi^2}\right)\sum_{n=1}^{\infty}\left(\frac{1}{n^2}\right)\exp\left[-\frac{D_i t \pi^2 n^2}{r_0^2}\right] \tag{9}$$

$$F = 1 + \left(\frac{6}{\pi^2}\right)\sum_{n=1}^{\infty}\left(\frac{1}{n^2}\right)\exp\left[-n^2 Bt\right] \tag{10}$$

where F is the fractional equilibrium at time t ($F = q_t/q_e$), q_e is the amount of adsorbate adsorbed at an infinite time (mg g^{-1}) and q_t is the amount of adsorbate adsorbed at a time t; Bt is the time constant; D_i is the effective diffusion coefficient of the dye, r_0 is the solid particle radius [59]. The Bt value was determined from Eq. (11), developed by Reichenberg [60].

$$\text{Bt} = -0{,}4977 - \ln\left(1 - F\right) \tag{11}$$

The Bt value is calculated for each F value and plotted as a function of t (Boyd's graph). If the graph is a straight line passing through the origin, then the adsorption rate is governed by the particle diffusion mechanism, otherwise, it is governed by the film diffusion.

Figs. 6a and b represent the graphs of qt vs. $t_{1/2}$ for the dye adsorption onto the BCP and BCK respectively. It is observed that the experimental data do not behave linearly and do not pass through the origin. The Webber and Morris model suggest that, if the first straight segment (adsorption initial stage) has a linear coefficient different from zero, the intra-particle diffusion isn't the limiting step, so the process that controls the adsorption can be the diffusion in the film [57]. As shown in Table 3, the lower value

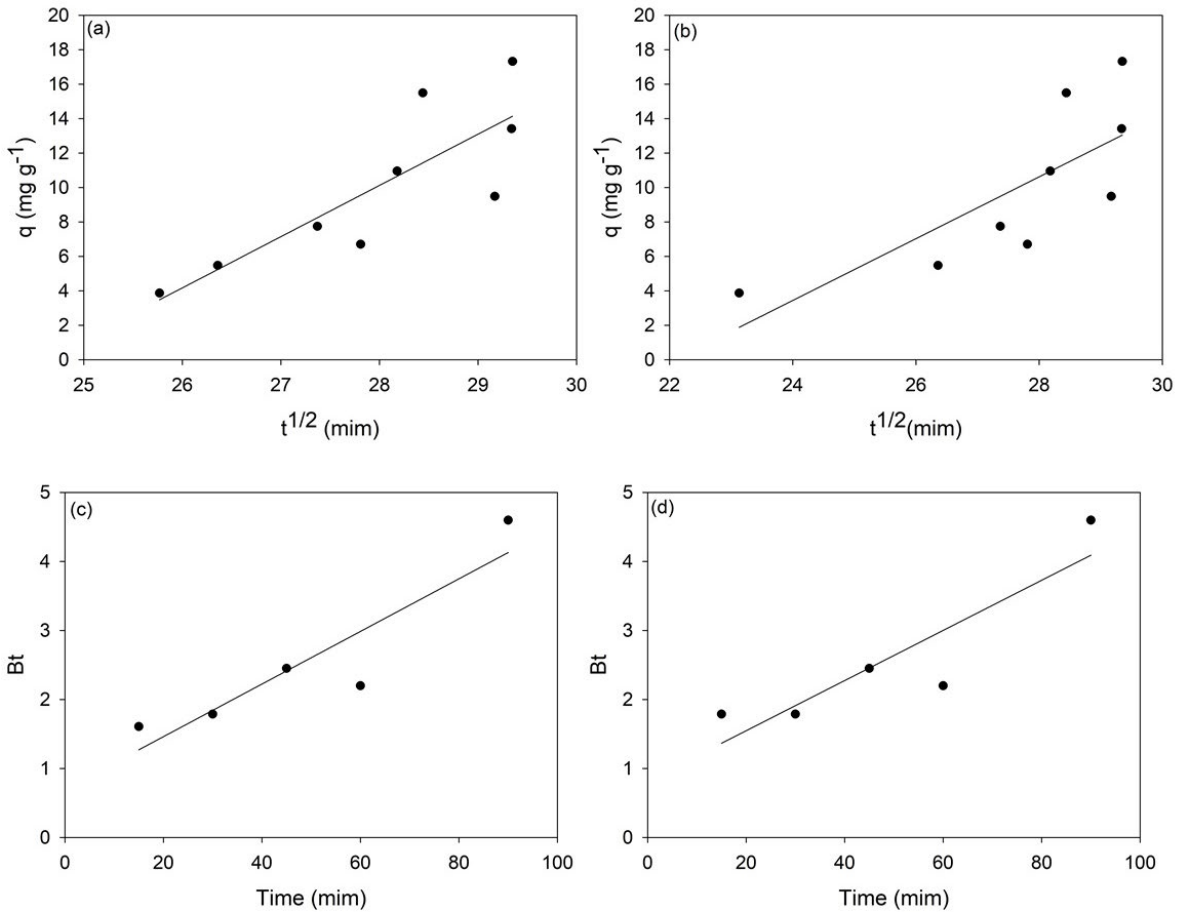

Fig. 6. Adjustment of the Weber and Morris model applied to adsorption of dianix dye CC in BCP (a) and BCK (b), and Boyd intraparticle diffusion model for BCP (c) and BCK (d): (•) experimental data and (–) adjusted model.

of the *C* constant for the BCK sample shows that the boundary layer effect in the diffusion process of the dye in this porous material is going to be smaller, since the constant *C* gives an idea of the thickness of it. The dye adsorption equilibrium was reached more rapidly in the BCK rather than BCP, due to its lower diffusion coefficient (K_{ad}) at this step. The fit of the Boyd model is shown in Figs. 6c and d. Again, the intra-particle diffusion was not the stage that limits the dye removal process over time, confirming the results obtained by the Weber and Morris model, once the line did not pass through the origin. This result suggests a greater resistance to mass transfer in the film around the adsorbent rather than the pores [61]. The transport through the film is usually the limiting step for systems presenting a high affinity between solute and biochar [54].

The effective diffusion coefficients of the royal dianix CC blue dye in the biochars were estimated from a mathematical model obtained from the fluid phase mass balance and adsorbent. The kinetic data were used to determine this parameter, and the following hypotheses were considered for the construction of the model:

- Constant diffusion coefficient;
- Isothermal process;
- Spherical particle;
- Mass transfer resistance of the liquid film is negligible;

By performing a solid phase mass balance [62]:

$$\frac{\partial q}{\partial t} = \frac{1}{r^2}\frac{\partial}{\partial r}\left(r^2 D_i \frac{\partial q}{\partial r}\right) \tag{12}$$

The initial and boundary conditions were as follows:

$$q(r,0) = q_0$$

$$q(r_c,t) = q_0$$

$$\left(\frac{\partial q}{\partial r}\right)_{r=0} = 0$$

The resolution of the diffusion Eq. (12) is given by Eq. (10) [62]. The model parameters were estimated, minimizing the objective function by the Marquardt method.

$$F = 1 + \left(\frac{6}{\pi^2}\right)\sum_{n=1}^{\infty}\left(\frac{1}{n^2}\right)\exp\left[-\frac{D_i t \pi^2 n^2}{r_0^2}\right] \tag{13}$$

The effective diffusion coefficient of the royal dianix CC blue in the adsorbent and the BCP and BCK was 1.55×10^{-16} cm^2 min^{-1} and 7.32×10^{-16} cm^2 min^{-1} respectively. These results confirm that the dye adsorption equilibrium in the sample BCK was reached faster when compared to BCP, once it exhibited a higher diffusion coefficient. This behavior may be due to the lower S_g value of biochar BCK which implies a shorter time for the mass transfer process to reach equilibrium. In addition, the larger mean diameter of the pores may favor the dye diffusion into the pores, thus reaching equilibrium faster, once the diffusion is facilitated in materials with less compact porous structures [4,7].

The knowledge of the adsorption equilibrium is the initial step to study the behavior of an adsorbent in a separation process. The isotherms are useful for describing the adsorption capacity, selecting the most suitable adsorbent, as well as establishing the required amounts in a given application. In addition, it is also a powerful tool for a theoretical study and interpretation of thermodynamic parameters, such as heat of adsorption [9,48,63].

The biochar adsorption capacity was evaluated, and the Langmuir and Freundlich non-linear models were adjusted to the experimental data at different temperatures. The Langmuir isotherm [Eq. (14)] proposes an adsorption mechanism on homogeneous surfaces, assuming uniformity of adsorbent surface, and all the active adsorption sites are energetically identical [64]. The Freundlich isotherm [Eq. (15)] is an empirical equation that can be applied to heterogeneous systems [65].

$$q = q_s \frac{bC_{eq}}{1 + bC_{eq}} \tag{14}$$

$$q = KC_{eq}^{1/n} \tag{15}$$

where q_s is the monolayer saturation capacity (mg g^{-1}), C_{eq} is the concentration in the liquid phase at equilibrium (mg L^{-1}); *b* is the adsorption equilibrium constant (L mg^{-1}); *K* is the Freundlich constant [(mg g^{-1}) (L mg^{-1})$^{1/n}$], and *n* is a constant (dimensionless) related to the adsorption intensity.

In Fig. 7 the adjustments of Langmuir and Freundlich nonlinear models to the experimental data at temperatures studied are shown. From the isothermal parameters summarized in Table 3, it can be observed that both models were adequately fitted to experimental data. When evaluating the q_s and b values, determined by the Langmuir model, the dye adsorption capacity onto the synthesized adsorbents decreased with the increase in temperature. This behavior may be due to the exothermic nature of the adsorption, once the increase in temperature of the medium favors the displacement of the mass transfer equilibrium to the liquid phase of the system. Higher temperatures increase the agitation rate of water molecules, increasing the available energy for solute-solvent binding. The higher solubility due to the increase in temperature of the system compromises the hydrophobic interactions between the dye and the biochar surface and favors the formation of ion interactions and hydrogen bonds [66]. Furthermore, the sample BCP presented a greater adsorption capacity when compared to the BCK. As shown in the physicochemical characterization of the adsorbents, the BCP is characterized as a material with a larger S_{BET} and total pore volume, consequently presenting a greater number of adsorption sites available to bind to the dye, thus favoring the adsorption. In addition, the chemical composition of the adsorbent surface also contributed decisively to the higher adsorptive capacity of the BCP. However, it is worth mentioning that the sample BCK showed good dye adsorption capacity despite its very low surface area, due to the interactions that occurred between the functional groups of the biochar surface and

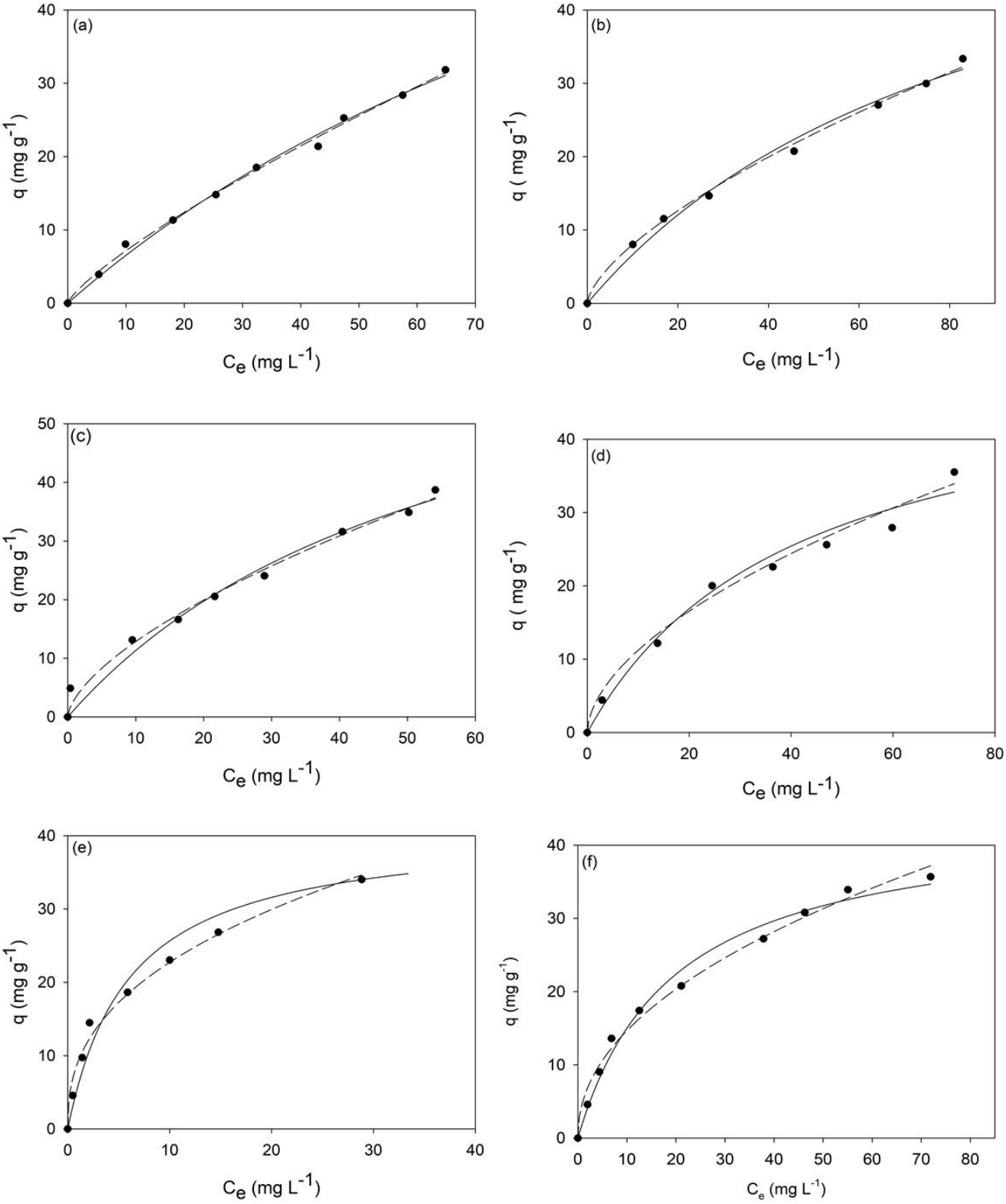

Fig. 7. Non-linear fits of Langmuir and Freundlich isotherm models to the dye adsorption onto biochars data: (a) BCP at 20°C, (b) BCK at 20°C, (c) BCP at 30°C, (d) BCK at 30°C, (e) BCP at 40°C, and (f) BCK at 40°C: (•) experimental data, (–) Langmuir and (– –) Freundlich (conditions: C_0 = 25–300 mg L^{-1}; pH: 7.0; T = 120 min).

Table 3
Isothermal parameters of Langmuir and Freundlich models for dye adsorption onto biochars

Model	Temperature	Parameters					
		q_s	b	K	n	R^2	RMSE
		BCP					
Langmuir	20	98.449	0.007	–	–	0.994	0.817
	30	77.054	0.017	–	–	0.978	1.839
	40	41.116	0.166	–	–	0.966	2.079
Freundlich	20	–	–	1.157	1.263	0.996	0.608
	30	–	–	2.995	1.581	0.988	1.325
	40	–	–	9.100	2.515	0.988	1.182
		BCK					
Langmuir	20	66.945	0.011	–	–	0.985	1.033
	30	51.483	0.024	–	–	0.985	1.644
	40	43.990	0.052	–	–	0.974	0.971
Freundlich	20	–	–	1.753	1.517	0.991	0.598
	30	–	–	3.090	1.785	0.980	1.432
	40	–	–	4.951	2.120	0.990	1.522

q_s (mg g^{-1}), b (L mg^{-1}) e a [(mg g^{-1}) (L mg^{-1})$^{1/n}$]

the dye molecules [67]. The adsorption capacity of biochar is due both to the molecular sieve effect (size and shape of carbon pores) and the chemical composition of the biochar surface [17]. As observed in the kinetic study, the film diffusion was a limiting step of the process, that is, both adsorbents showed a high affinity with the solute. Moreover, the n values, determined by the Freundlich model, showed that the adsorption of dye onto the biochars was favorable at all temperatures evaluated, due to the n values < 0.

3.4. Thermodynamics of adsorption

The dye adsorption thermodynamic parameters onto the biochar, such as Gibbs energy ($\Delta G°$), enthalpy ($\Delta H°$) and adsorption entropy ($\Delta S°$) were calculated using the following equations [5]:

$$\Delta G° = -RT \ln K_d \tag{16}$$

$$\Delta G° = \Delta H° - T\Delta S° \tag{17}$$

Combining the above two equations:

$$\ln k_d = -\frac{\Delta G°}{RT} - \frac{\Delta H°}{RT} + \frac{\Delta S°}{R} \tag{18}$$

where R is the universal gas constant (8.314 J mol^{-1} K^{-1}), and T is the temperature (K) and K_d is the thermodynamic equilibrium constant (L g^{-1}), which can be obtained by plotting q_e/C_e vs. q_e and extrapolating the curve when q_e tends to zero.

The results of the thermodynamic parameters of the royal dianix CC blue adsorption on the biochars BCP and BCK are shown in Table 4, with similar behavior for both carbons. Negative $\Delta G°$ values show that the transfer of the royal dianix CC blue dye from the solution to the adsorbent surface is a spontaneous process. In addition, the $\Delta G°$ values were more negative at 293 K, in which the adsorption capacity was higher, suggesting that the adsorption is more effective at this temperature [68]. However, these values become less negative with increasing temperature, due to the increase in energy of the system, which results in a reduction of enthalpy and an increase in entropy. The negative $\Delta H°$ values show an amount of energy released during the adsorption process, being the process exothermic and enthalpically driven. Negative enthalpy can be due to the predominance of strong interactions, such as hydrogen bonds and ion interactions between the dye and the biocarbon molecules. The adsorption process can be classified as physical or chemical adsorption, depending on the magnitude of the enthalpy change. $\Delta H°$ values between 5 and 40 kJ mol^{-1} are characteristic of physisorption, while higher values (40–800 kJ mol^{-1}) suggest chemisorption [69,70]. Therefore, the dye adsorption was of chemical nature for both biochars, as previously evidenced in the kinetic study. The negative adsorption entropy ($\Delta S°$) indicates an increase in the organization of the system, associated with the accommodation of the dye molecules in more ordered layers on the adsorbent surface [7].

4. Conclusion

The results that were obtained allowed to elucidate the mass transfer mechanisms involved in the adsorption of royal dianix CC dye in the biochars synthesized from the cupuaçu bark. The diffusion process controlling step in both adsorbents is the diffusion in the film. In addition, the equilibrium data indicated that the biochar with H_3PO_4 had a higher adsorption capacity than the biochar with KOH, a behavior explained by the different physical and chemical characteristics of the biochars. The activation with

Table 4
Thermodynamic parameters of royal dianix CC blue dye adsorption on BCP and BCK biochars

Sample	Temperature (k)	Parameters		
		$\Delta G°$ (kJ mol^{-1})	$\Delta H°$ (kJ mol^{-1})	$\Delta S°$ (kJ mol^{-1})
BCP	293	–23.28	–153.34	–0.44
	303	–21.22		
	313	–14.35		
BCK	293	–21.24	–75.32	–0.18
	303	–19.33		
	313	–17.55		

the was more effective in modifying the precursor structure, favoring the development of an adsorbent with a number of functional groups on its surface, greater superficial area, and the higher average volume of the pores and these characteristics are being favorable to the adsorption process. This study demonstrated that the cupuçu bark has the potential to be used as a PM in the synthesis of biochar, since the adsorbents that were produced had adequate adsorption capacity of the textile dye, and could be a promising alternative in the substitution of the commercial adsorbent matrix. Besides that, the use of residual biomass leads to a reduction in the environmental impact that comes from the inappropriate disposal of these wastes in nature.

Acknowledgment

The authors acknowledge CETENE by analysis, the FAPESB, CNPq and CAPES- Brazil (Finance Code 001) for financial support.

References

[1] A.A. Inyinbor, F.A. Adekola, G.A. Olatunji, Kinetics, isotherms and thermodynamic modeling of liquid phase adsorption of Rhodamine B dye onto *Raphia hookerie* fruit epicarp, Water Res., 15 (2016) 14–27.
[2] Z.U. Ahmad, L.G. Yao, J. Wang, D.D. Gang, F. Islam, Q.Y. Lian, M.E. Zappi, Neodymium embedded ordered mesoporous carbon (OMC) for enhanced adsorption of sunset yellow: characterizations, adsorption study and adsorption mechanism, Chem. Eng. J., 359 (2019) 814–826.
[3] K. Gayathri, N. Palanisamy, Methylene blue adsorption onto an eco-friendly modified polyacrylamide/graphite composites: investigation of kinetics, equilibrium, and thermodynamic studies, Sep. Sci. Technol., 55 (2020) 266–277.
[4] Z. Harrache, M. Abbas, T. Aksil, M. Trari, Thermodynamic and kinetics studies on adsorption of Indigo Carmine from aqueous solution by activated carbon, Rev. Microchem., 144 (2019) 180–189.
[5] A. Kumar, H.M. Jena, Removal of methylene blue and phenol onto prepared activated carbon from Fox nutshell by chemical activation in batch and fixed-bed column, J. Cleaner Prod., 137 (2016) 1246–1259.
[6] M.N. Mahamad, M.A.A. Zaini, Z.A. Zakaria, Preparation and characterization of activated carbon from pineapple waste biomass for dye removal, Int. Biodeterior. Biodegrad., 102 (2015) 274–280.
[7] M.J.P. Brito, C.M. Veloso, L.S. Santos, R.C.F. Bonomo, R. da Costa Ilhéu Fontan, Adsorption of the textile dye Dianix® royal blue CC onto carbons obtained from yellow mombin fruit stones and activated with KOH and H_3PO_4: kinetics, adsorption equilibrium and thermodynamic studies, Powder Technol., 339 (2018) 334–343.
[8] S.V. Lacerda, J.B. López-Sotelo, A. Correa-Guimarães, S. Hernández-Navarro, M. Sánchez-Báscones, L.M. Navas-Gracia, P. Martín-Ramos, J. Martín-Gil, Rhodamine B removal with activated carbons obtained from lignocellulosic waste, J. Environ. Manage., 155 (2015) 67–76.
[9] C. Xu, W.-Z. Sun, X.-L. Qin, Y.-X. Jia, S.-T. Yu, M. Xian, Effective adsorption of phenolic compounds by functional group modified resins: behavior and mechanism, Sep. Sci. Technol., 54 (2019) 467–477.
[10] M.J.P. Brito, C.M. Veloso, R.C.F. Bonomo, R. da Costa Ilhéu Fontan, L.S. Santos, K.A. Monteiro, Activated carbons preparation from yellow mombin fruit stones for lipase immobilization, Fuel Process. Technol., 156 (2017) 421–428.
[11] E. Vunain, T. Biswick, Adsorptive removal of methylene blue from aqueous solution on activated carbon prepared from Malawian baobab fruit shell wastes: equilibrium, kinetics and thermodynamic studies, Sep. Sci. Technol., 54 (2018) 27–41.
[12] S.N. Andrade, C.M. Veloso, R.C.I. Fontan, R.C.F. Bonomo, L.S. Santos, M.J.P. Brito, G.A. Diniz, Chemical-activated carbon from coconut (*Cocos nucifera*) endocarp waste and its application in the adsorption of β-lactoglobulin protein, Rev. Mex. Ing. Quím., 17 (2018) 441–453.
[13] S. Rangabhashiyam, P. Balasubramanian, The potential of lignocellulosic biomass precursors for biochar production: performance, mechanism and wastewater application—a review, Ind. Crops Prod., 128 (2019) 405–423.
[14] A.B. Azadeh, D.G. Allen, C.Q. Jia, Benefits of microwave heating method in production of activated carbon, Can. J. Chem. Eng., 94 (2016) 1262–1268.
[15] A. Castro-Muñiz, S. Lorenzo-Fierro, A. Martínez-Alonso, J.M.D. Tascón, V. Fierro, F. Suárez-García, J.I. Paredes, Ordered mesoporous carbons obtained from low-value coal tar products for electrochemical energy storage and water remediation, Fuel Process. Technol., 196 (2019) 106–152.
[16] R.G. Pereira, C.M. Veloso, N.M. da Silva, L.F. de Sousa, R.C.F. Bonomo, A.O. de Souza, M.O. da Guarda Souza, R. da Costa Ilhéu Fontan, Preparation of activated carbons from cocoa shells and siriguela seeds using H_3PO_4 and $ZnCL_2$ as activating agents for BSA and α-lactalbumin adsorption, Fuel Process. Technol., 126 (2014) 476–486.
[17] P. González-García, Activated carbon from lignocellulosics precursors: a review of the synthesis methods, characterization techniques and applications, Renewable Sustainable Energy Rev., 82 (2018) 1393–1414.
[18] J.N. da Cruz, D.C. Pimenta, R.L. de Melo, J.R.O. Nascimento, Isolation and biochemical characterisation of angiotensin-converting enzyme inhibitory peptides derived from the enzymatic hydrolysis of cupuassu seed protein isolate, J. Funct. Foods, 27 (2016) 104–114.
[19] N.F. Cardoso, E.C. Lima, I.S. Pinto, C.V. Amavisca, B. Royer, R.B. Pinto, W.S. Alencar, S.F.P. Pereira, Application of cupuassu shell as biosorbent for the removal of textile dyes from aqueous solution, J. Environ. Manage., 92 (2011) 1237–1247.

[20] M.P.F. Santos, M.J.P. Brito, E.C.S. Junior, R.C.F. Bonomo, C.M. Veloso, Pepsin immobilization on biochar by adsorption and covalent binding, and its application for hydrolysis of bovine casein, J. Chem. Technol. Biotechnol., 94 (2019) 1982–1990.
[21] P.J. van Soest, J.B. Robertson, B.A. Lewis, Methods for dietary fiber, neutral detergent fiber, and nonstarch polysaccharides in relation to animal nutrition, J. Dairy Sci., 74 (1991) 3583–3597.
[22] AOAC, AOAC Official Methods of Analysis, Vol. 16, Association of Official Analytical Chemistry, Arlington, 1995.
[23] J.R. Regalbuto, J. Robles, The Engineering of Pt/Carbon Catalyst Preparation University of Illinois, Catalysis Laboratory, University of Illinois at Chicago, Chicago, 2004.
[24] P.D. Muley, C. Henkel, K.K. Abdollahi, C. Marculescu, D. Boldor, A critical comparison of pyrolysis of cellulose, lignin, and pine sawdust using an induction heating reactor, Energy Convers. Manage., 117 (2016) 273–280.
[25] G. Selvaraju, N. Kartini Abu Bakar, Production of a new industrially viable green-activated carbon from *Artocarpus integer* fruit processing waste and evaluation of its chemical, morphological and adsorption properties, J. Cleaner Prod., 141 (2017) 989–999.
[26] V. Fierro, V. Torné-Fernández, A. Celzard, Kraft lignin as a precursor for microporous activated carbons prepared by impregnation with ortho-phosphoric acid: synthesis and textural characterization, Microporous Mesoporous Mater., 92 (2006) 243–250.
[27] W.C. Lim, C. Srinivasakannan, N. Balasubramanian, Activation of palm shells by phosphoric acid impregnation for high yielding activated carbon, J. Anal. Appl. Pyrolysis, 88 (2010) 181–186.
[28] M.A. Lillo-Ródenas, J. Juan-Juan, D. Cazorla-Amorós, A. Linares-Solano, About reactions occurring during chemical activation with hydroxides, Carbon, 42 (2004) 1371–1375.
[29] B. Acevedo, C. Barriocanal, Texture and surface chemistry of activated carbons obtained from tyre wastes, Fuel Process. Technol., 134 (2015) 275–283.
[30] Y.Y. Sun, H. Li, G.C. Li, B.Y. Gao, Q.Y. Yue, X.B. Li, Characterization and ciprofloxacin adsorption properties of activated carbons prepared from biomass wastes by H_3PO_4 activation, Bioresour. Technol., 217 (2016) 239–244.
[31] C.P. da Silva, A.V. dos Santos, A.S. Oliveira, M.O. da Guarda Souza, Synthesis of composites and study of the thermal behavior of sugarcane bagasse/iron nitrate mixtures in different proportions, J. Therm. Anal. Calorim., 131 (2017) 611–620.
[32] Y.P. Guo, D.A. Rockstraw, Physicochemical properties of carbons prepared from pecan shell by phosphoric acid activation, Bioresour. Technol., 98 (2007) 1513–1521.
[33] F. Marrakchi, M. Auta, W.A. Khanday, B.H. Hameed, High-surface-area and nitrogen-rich mesoporous carbon material from fishery waste for effective adsorption of methylene blue, Powder Technol., 321 (2017) 428–434.
[34] Z. Movasaghi, B. Yan, C. Niu, Adsorption of ciprofloxacin from water by pretreated oat hulls: equilibrium, kinetic, and thermodynamic studies, Ind. Crops Prod., 127 (2019) 237–250.
[35] M.A. Nahil, P.T. Williams, Pore characteristics of activated carbons from the phosphoric acid chemical activation of cotton stalks, Biomass Bioenergy, 37 (2012) 142–149.
[36] H. Marsh, F. Rodríguez-Reinoso, Activation Processes (Chemical), Elsevier B.V., Amsterdam, Holland, 2006, p. 322.
[37] M. Jagtoyen, F. Derbyshire, Activated carbons from yellow poplar and white oak by H_3PO_4 activation, Carbon, 36 (1998) 1085–1097.
[38] L.R. Radovic, F. Rodriguez-Reinoso, Chemistry and Physics of Carbon, Marcel Dekker, New York, 1997.
[39] C.R. Correa, T. Otto, A. Kruse, Influence of the biomass components on the pore formation of activated carbon, Biomass Bioenergy, 97 (2017) 53–64.
[40] A. Elmouwahidi, E. Bailón-García, A.F. Pérez-Cadenas, F.J. Maldonado-Hódar, F. Carrasco-Marín, Activated carbons from KOH and H_3PO_4-activation of olive residues and its application as supercapacitor electrodes, Electrochim. Acta, 229 (2017) 219–228.
[41] N. Rambabu, B.V.S.K. Rao, V.R. Surisetty, U. Das, A.K. Dalai, Production, characterization, and evaluation of activated carbons from de-oiled canola meal for environmental applications, Ind. Crops Prod., 67 (2015) 572–581.
[42] S.J. Li, K.H. Han, J.X. Li, M. Li, C.M. Lu, Preparation and characterization of super activated carbon produced from gulfweed by KOH activation, Microporous Mesoporous Mater., 243 (2017) 291–300.
[43] C.C. Small, Z. Hashisho, A.C. Ulrich, Preparation and characterization of activated carbon from oil sands coke, Fuel, 92 (2012) 69–76.
[44] C.H. Xiong, Y.L. Li, G.T. Wang, L. Fang, S.G. Zhou, C.P. Yao, Q. Chen, X.M. Zheng, D.M. Qi, Y.Q. Fu, Y.F. Zhu, Selective removal of Hg(II) with polyacrylonitrile-2-amino-1,3,4-thiadiazole chelating resin: batch and column study, Chem. Eng. J., 259 (2015) 257–265.
[45] K.C. Bedin, A.C. Martins, A.L. Cazetta, O. Pezoti, V.C. Almeida, KOH-activated carbon prepared from sucrose spherical carbon: adsorption equilibrium, kinetic and thermodynamic studies for Methylene Blue removal, Chem. Eng. J., 286 (2016) 476–484.
[46] Q. Zhou, Y.-F. Duan, Y.-G. Hong, C. Zhu, M. She, J. Zhang, H.-Q. Wei, Experimental and kinetic studies of gas-phase mercury adsorption by raw and bromine modified activated carbon, Fuel Process. Technol., 134 (2015) 325–332.
[47] A. Rahmani-Sani, A. Hosseini-Bandegharaei, S.-H. Hosseini, K. Kharghani, H. Zarei, A. Rastegar, Kinetic, equilibrium and thermodynamic studies on sorption of uranium and thorium from aqueous solutions by a selective impregnated resin containing carminic acid, J. Hazard. Mater., 286 (2015) 152–163.
[48] H. Demiral, C. Güngör, Adsorption of copper(II) from aqueous solutions on activated carbon prepared from grape bagasse, J. Cleaner Prod., 124 (2016) 103–113.
[49] P.M. Pimentel, G. González, M.F.A. Melo, D.M.A. Melo, C.N. Silva Jr., A.L.C. Assunção, Removal of lead ions from aqueous solution by retorted shale, Sep. Purif. Technol., 56 (2007) 348–353.
[50] M.C. Ncibi, B. Mahjoub, M. Seffen, Investigation of the sorption mechanisms of metal-complexed dye onto *Posidonia oceanica* (L.) fibres through kinetic modelling analysis, Bioresour. Technol., 99 (2008) 5582–5589.
[51] S.S. Gupta, K.G. Bhattacharyya, Kinetics of adsorption of metal ions on inorganic materials: a review, Adv. Colloid Interface Sci., 162 (2011) 39–58.
[52] W.J. Weber, J. Carrell Morris, Kinetics of adsorption on carbon from solution, J. Sanitary Eng. Div. ASCE, 89 (1963) 31–60.
[53] G.E. Boyd, A.W. Adamson, L.S. Myers Jr., The exchange adsorption of ions from aqueous solution by organic zeolites. II. Kinetics, J. Am. Chem. Soc., 69 (1947) 2836.
[54] M. Sarkar, P.K. Acharya, B. Bhattacharya, Modeling the adsorption kinetics of some priority organic pollutants in water from diffusion and activation energy parameters, J. Colloid Interface Sci., 266 (2003) 28–32.
[55] T.A. Cigu, S. Vasiliu, S. Racovita, C. Lionte, V. Sunel, M. Popa, C. Cheptea, Adsorption and release studies of new cephalosporin from chitosan-*g*-poly(glycidyl methacrylate) microparticles, Eur. Polym. J., 82 (2016) 131–152.
[56] D. Mohan, K.P. Singh, V.K. Singh, Trivalent chromium removal from wastewater using low cost activated carbon derived from agricultural waste material and activated carbon fabric cloth, J. Hazard. Mater., 135 (2006) 280–295.
[57] J.J. João, W.S. Júnior, J.L. Vieira, Use of zeolite synthesized from coal ashl from Santa Catarina for removal of iron, manganese and methylene blue dye in water, Rev. Ambient. Agua, 13 (2018) 2224.
[58] G.E. do Nascimento, N.F. Campos, J.J. da Silva, C.M.B. de Menezes Barbosa, M.M.M.B. Duarte, Adsorption of anionic dyes from an aqueous solution by banana peel and green coconut mesocarp, Desal. Water Treat., 57 (2015) 1–16.
[59] R. Aravindhan, J.R. Rao, B.U. Nair, Kinetic and equilibrium studies on biosorption of basic blue dye by green macro algae *Caulerpa scalpelliformis*, J. Environ. Sci. Health. Part A Toxic/Hazard. Subst. Environ. Eng., 42 (2007) 621–631.

[60] D. Reichenberg, Properties of ion-exchange resin in relation to their structure. III. Kinetics of exchange, J. Am. Chem. Soc., 75 (1953) 589.
[61] G.M. Maciel, C.G.M. de Souza, C.A.V. de Araújo, E. Bona, C.W.I. Haminiuk, R. Castoldi, A. Bracht, R.M. Peralta, Biosorption of herbicide picloram from aqueous solutions by live and heat-treated biomasses of *Ganoderma lucidum* (Curtis) P. Karst and *Trametes* sp., Chem. Eng. J., 215 (2013) 331–338.
[62] D.M. Ruthven, Principles of Adsorption and Adsorption Process, John Wiley & Sons, New York, 1984.
[63] Ö. Gerçel, Biosorption of a basic dye from aqueous solutions by *Euphorbia rigida*, Sep. Sci. Technol., 43 (2008) 192–211.
[64] N. Ünlü, M. Ersoz, Adsorption characteristics of heavy metal ions onto a low cost biopolymeric sorbent from aqueous solutions, J. Hazard. Mater., 136 (2006) 272–280.
[65] Y.G. Chen, R.Q. Huang, C.M. Zhu, D.B. Wu, Y.H. Sun, Y. He, W.M. Ye, Adsorptive removal of La(III) from aqueous solutions with 8-hydroxyquinoline immobilized GMZ bentonite, J. Radioanal. Nucl. Chem., 299 (2014) 665–674.
[66] S.D. Khattri, M.K. Singh, Colour removal from synthetic dye wastewater using a bioadsorbent, Water Air Soil Pollut., 120 (2000) 283–294.
[67] A.R. Khataee, F. Vafaei, M. Jannatkhah, Biosorption of three textile dyes from contaminated water by filamentous green algal *Spirogyra* sp.: kinetic, isotherm and thermodynamic studies, Int. Biodeterior. Biodegrad., 83 (2013) 33–40.
[68] X.Y. Li, D. Han, M.Y. Zhang, B. Li, Z.B. Wang, Z.Q. Gong, P.K. Liu, Y.K. Zhang, X.H. Yang, Removal of toxic dyes from aqueous solution using new activated carbon materials developed from oil sludge waste, 578 (2019) 123505.
[69] R. Gonzalez-Olmos, M. Iglesias, Thermodynamics and kinetics of fuel oxygenate adsorption into granular activated carbon, J. Chem. Eng. Data, 53 (2008) 2556–2561.
[70] X. Wang, J.M. Pan, W. Guan, J.D. Dai, X.H. Zou, Y.S. Yan, C.X. Li, W. Hu, Selective removal of 3-chlorophenol from aqueous solution using surface molecularly imprinted microspheres, J. Chem. Eng. Data, 56 (2011) 2793–2801.